

See discussions, stats, and author profiles for this publication at: <https://www.researchgate.net/publication/231371869>

Single Event Kinetic Modeling of the Methanol-to-Olefins Process on SAPO-34

ARTICLE *in* INDUSTRIAL & ENGINEERING CHEMISTRY RESEARCH · JULY 2004

Impact Factor: 2.59 · DOI: 10.1021/ie040041u

CITATIONS

52

READS

199

2 AUTHORS, INCLUDING:



Gilbert F. Froment

Texas A&M University

85 PUBLICATIONS 4,022 CITATIONS

SEE PROFILE

Single Event Kinetic Modeling of the Methanol-to-Olefins Process on SAPO-34

Saeed M. Alwahabi[†] and Gilbert F. Froment*

Chemical Engineering Department, Texas A&M University, College Station, Texas 77843-3122

The MTO process on SAPO-34 was modeled in a fundamental way using the single event concept combined with the Evans–Polanyi relationship. This approach together with a number of thermodynamic constraints leads to a drastic reduction of the number of independent parameters. These were determined from the experimental data using a combination of a hybrid genetic algorithm, sequential quadratic programming, and the Levenberg–Marquardt optimizer. The effect of the structure of reactant and product on the rate coefficients of the various types of elementary steps was illustrated. The effect of operating variables such as temperature and the methanol partial pressure was investigated using the kinetic model. The deactivation of the catalyst was modeled in terms of the amount of C₆₊ olefins formed and trapped inside the SAPO-34 cavities. The effect of deactivation on the evolution with process time of the conversion and product yields of the MTO process was illustrated by the simulation of an isothermal fixed bed reactor.

1. Introduction

The availability of huge quantities of natural gas has led to an increased interest in the catalytic methanol-to-olefins (MTO) process as an alternative for the thermal cracking process for olefins production. Commercialization seems close now. Vora et al.¹ have provided information on the technological aspects, while Froment et al.² have reviewed catalytic aspects.

The development of a realistic kinetic model for a process of this type requires detailed information on the mechanism of the reactions. The MTO reaction network consists of hundreds of elementary steps however, and this has led researchers to model the methanol conversion by drastic lumping of reactions and reacting species. Considering the methanol reaction over ZSM-5 as autocatalytic, Chen and Reagan³ developed a four-lump model, while Schoenfelder et al.⁴ described the process in terms of seven lumps: oxygenates, ethylene, propylene, butylene, paraffins, methane, carbon monoxide, hydrogen, and water. Bos and Tromp⁵ developed a kinetic model for the MTO process based on SAPO-34. The final reaction scheme consisted of 12 reactions involving six product lumps plus coke. Some of the reactions were of the first order; others were of the second order. By their very nature, lumped kinetic models cannot predict the detailed product composition, and the estimated rate and equilibrium coefficients generally turn out to be dependent on feed composition and reaction conditions.

In the present work, the rate coefficients of the elementary steps involved in the MTO network have been modeled in terms of the single event kinetics approach introduced by Froment and co-workers,⁶ combined with the Evans–Polanyi relation. This funda-

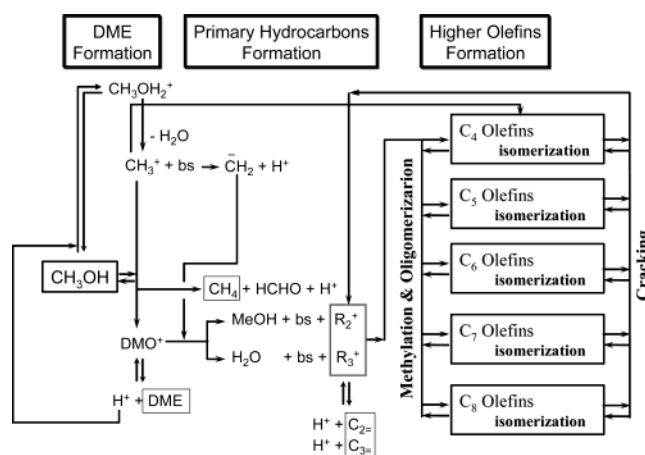


Figure 1. Reaction scheme for the MTO process.¹⁰

mental procedure provides a very substantial reduction of the number of parameters to be estimated.

2. Reaction Scheme

2.1. Formation of DME and Primary Olefins.


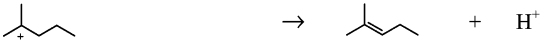



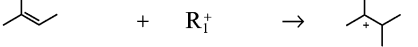
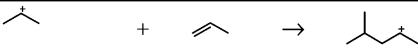
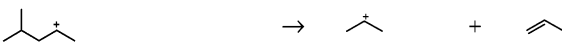
Recently, Park and Froment^{7,8} performed a kinetic modeling for the MTO process on a ZSM-5 catalyst. Eight rival mechanisms were considered. After discrimination between these, the surface-bonded oxonium methylene mechanism proposed by Hutchings et al.⁹ was retained. According to this mechanism, represented schematically in Figure 1,¹⁰ proton transfer from the surface methoxy to a nearby basic zeolite site (e.g., an adjacent Al–O site) yields a surface-bonded oxonium methylene (CH_2^+) that reacts with protonated dimethyl ether (DMO^+) to produce a surface-bonded ethyl and/or propyl carbenium ions (R_2^+ , R_3^+). Deprotonation of R_2^+ and R_3^+ forms gas-phase ethylene and propylene, respectively. In the present work, the surface-bonded oxonium methylene mechanism is adopted for the kinetic modeling of the primary hydrocarbon formation.

2.2. Formation of Higher Olefins. In MTO, as in any hydrocarbon transformation on heterogeneous acid

* To whom correspondence should be addressed. Tel.: (979) 845-3361. Fax: (979) 845-6446. E-mail: g.froment@ChE.tamu.edu.

[†] Present address: SABIC R&T, Riyadh 11551, Saudi Arabia.

Table 1. Types of Elementary Steps Involved in the Formation of Higher Olefins

Elementary Step	Example
Protonation	
Deprotonation	
Hydride Shift	
Methyl Shift	
PCP Branching	
Methylation	
Oligomerization	
β -scission	

catalysts, the conversion of the primary products to higher hydrocarbons proceeds via carbenium ion mechanisms. Methylation of surface carbenium ions, oligomerization, and cracking via β -scission are typical elementary steps increasing or decreasing the number of carbon atoms in the produced olefins.

Within the same number of carbon atom, the structure of the carbenium ions is modified by various types of rearrangement, including methyl shift and protonated cyclopropane (PCP) branching. As a result, almost all olefin isomers can be formed by deprotonation of those carbenium ions. Table 1 contains the elementary steps describing the formation of higher olefins with carbenium ions as intermediates.

With longer methanol space times (i.e., higher methanol conversion), the olefins are converted into paraffins and aromatics. The formation of these products is generally explained in terms of hydride transfer followed by cyclization of olefinic carbenium ions. The present study focuses on the reaction network corresponding to conditions where the amount of paraffins and aromatics is negligible. This is almost always true for SAPO-34 and true for ZSM-5 at moderate methanol conversion.

3. Kinetic Modeling of Olefins Formation in Terms of Elementary Steps and Single Events

3.1. Construction of Reaction Network. As discussed above, the MTO process can be divided into three stages; (i) the formation of dimethyl ether, (ii) the formation of the primary hydrocarbons, and (iii) the conversion of the primary products into higher olefins.

Table 2 shows the elementary steps describing the formation of the primary products. These steps involve surface-bonded oxonium methyl ylide and protonated DME.

The reaction network for the formation of higher olefins is much more complicated and contains a large

Table 2. Elementary Steps Involved in the Formation of Primary Products of the MTO Process

elementary steps	rate or equilibrium constants
DME Formation	
$\text{MeOH} + \text{H}^+ \rightleftharpoons \text{MeOH}_2^+$	$K_{\text{pr}}(\text{MeOH})$
$\text{MeOH}_2^+ \rightleftharpoons \text{R}_1^+ + \text{H}_2\text{O}$	$K_{\text{F}}(\text{R}_1^+), K_{\text{C}}(\text{R}_1^+)$
$\text{R}_1^+ + \text{MeOH} \rightleftharpoons \text{DMO}^+$	$K_{\text{F}}(\text{DMO}^+), K_{\text{C}}(\text{DMO}^+)$
$\text{DMO}^+ \rightleftharpoons \text{DME} + \text{H}^+$	$K_{\text{pr}}(\text{DME})$
Methane Formation	
$\text{R}_1^+ + \text{MeOH} \rightarrow \text{CH}_4 + \text{HCHO} + \text{H}^+$	$K_{\text{F}}(\text{CH}_4)$
Primary Olefins Formation	
$\text{R}_1^+ + \text{bs} \rightleftharpoons \text{OM} + \text{H}^+$	$K_{\text{sr}}(\text{R}_1^+; \text{bs}), K_{\text{sr}}(\text{OM}; \text{H}^+)$
$\text{OM} + \text{DMO}^+ \rightarrow \text{R}_2^+ + \text{MeOH} + \text{bs}$	$K_{\text{sr}}(\text{OM}; \text{DMO}^+; \text{R}_2^+)$
$\text{R}_2^+ \rightleftharpoons \text{O}_2 + \text{H}^+$	$K_{\text{de}}(\text{R}_2^+), K_{\text{pr}}(\text{O}_2)$
$\text{OM} + \text{DMO}^+ \rightarrow \text{R}_3^+ + \text{H}_2\text{O} + \text{bs}$	$K_{\text{sr}}(\text{OM}; \text{DMO}^+; \text{R}_3^+)$

number of elementary steps. To generate the network for such complex processes, Froment and co-workers^{11–15} developed a computer algorithm characterizing the various species by Boolean relation matrices and vectors. Park and Froment^{7,8} utilized this algorithm for the generation of the MTO reaction network on ZSM-5. The network thus generated is adapted for the development of the kinetic model for the MTO reaction on SAPO-34. For a network extending to C₈, the number of elementary steps and species generated by the computer algorithm are given in Table 3.

The same number of elementary steps and the same products are used for the SAPO-34 based process as for MTO on ZSM-5. It is true that heavy components that are detected with ZSM-5 do not show up among the products obtained with SAPO-34; nevertheless, they are actually formed but trapped inside the SAPO-34 cavities.

3.2. Formulation of the Rate Equations. The kinetic equations for the formation of the primary products and the higher olefins are based on the

Table 3. Number of Elementary Steps and Species Involved in the Reaction Network⁷

Number of Species	
olefins	142
carbenium ions	83
total	225
Number of Elementary Steps	
protonation	142
deprotonation	142
hydride shift	88
methyl shift	42
PCP branching	151
methylation	88
oligomerization	52
β -scission	21
total	726

reaction mechanism presented in Figure 1. The olefin isomers were shown to be in equilibrium, so that their partial pressures can be obtained from the composition of the equilibrium mixture. For an elementary step in which the adsorbed species have reached pseudo-equilibrium, the concentration of the adsorbed species were calculated using the classical Hougen–Watson formalism. If not, the pseudo-steady-state approximation was used instead. The elementary steps of protonation–deprotonation and the various rearrangements were considered to reach equilibrium. Yet, it is important to take them into account because the surface concentrations of the carbenium ions involved in the kinetic model are determined by these steps.

The number of rate and equilibrium coefficients required for the calculation of the rate expressions for the various products amounts to 253. This means that, accounting for the temperature dependency of these rate and equilibrium coefficients, 504 parameters need to be estimated. The majority of these parameters come from the detailed reaction network generated by the computer algorithm for the higher olefins production.

3.3. Modeling of Rate Coefficients and Equilibrium Constants. *3.3.1. Single Event Concept.* It would be unrealistic to expect a smooth estimation procedure and significant values for the parameters when the model contains such a large number of them. A reduction in the number of parameters is required. For this reason, Froment and co-workers introduced the concept of “single event”.⁶ The concept factors out the structure effect from the change of standard entropy associated with the transformation of a reactant into a product through an activated complex. From transition state theory, the rate coefficient can be written as:

$$K = \frac{k_B T}{h} \exp\left(\frac{\Delta S^{\circ\dagger}}{R}\right) \exp\left(-\frac{\Delta H^{\circ\dagger}}{RT}\right) \quad (1)$$

According to statistical thermodynamics, the standard entropy of a species is determined by several contributions associated with the various motions of the species such as translation, vibration, and rotation. The latter is composed of two terms: the intrinsic value (\hat{S}°) and a term due to symmetry (σ), which depends on the geometry of the molecule:

$$S_{\text{rot}}^\circ = \hat{S}_{\text{rot}}^\circ - R \ln(\sigma) \quad (2)$$

Accounting for the effect of chirality, the rotational contribution S_{rot}° is given by:

$$S_{\text{rot}}^\circ = \hat{S}_{\text{rot}}^\circ - R \ln\left(\frac{\sigma}{2^n}\right) \quad (3)$$

where n is the number of chiral centers in a species. The expression in the parentheses that quantifies all symmetry contributions of a species is called the global symmetry number and is represented further by σ_{gl} .

The difference in standard entropy between reactant and activated complex due to symmetry changes is given by

$$\Delta S_{\text{sym}}^{\circ\dagger} = R \ln\left(\frac{\sigma_{\text{gl}}^r}{\sigma_{\text{gl}}^\ddagger}\right) \quad (4)$$

Substituting this contribution into eq 1 leads to

$$K = \left(\frac{\sigma_{\text{gl}}^r}{\sigma_{\text{gl}}^\ddagger}\right) \frac{k_B T}{h} \exp\left(\frac{\Delta \hat{S}^{\circ\dagger}}{R}\right) \exp\left(-\frac{\Delta H^{\circ\dagger}}{RT}\right) \quad (5)$$

The rate coefficient of the elementary step (K) can now be written as a multiple of that of a single event, \tilde{k} :

$$K = n_e \tilde{k} \quad (6)$$

The number of single events (n_e) is the ratio of the global symmetry numbers of the reactant and the activated complex:

$$n_e = \frac{\sigma_{\text{gl}}^r}{\sigma_{\text{gl}}^\ddagger} \quad (7)$$

A single event frequency factor that does not depend on the structure of the reactant and activated complex and is unique for a given type of elementary step can be defined as

$$\tilde{A} = \frac{k_B T}{h} \exp\left(\frac{\Delta S^\circ}{R}\right) \quad (8)$$

Since the effect of a difference in structure between the reactant and the activated complex has been factored out by introducing the number of single events, the single event rate coefficient now truly characterizes the reaction step itself at the fundamental level. The calculation of the global symmetry numbers of the reacting and produced carbenium ion and of the activated complex requires their configuration. These can be determined by means of quantum chemical packages such as MOPAC, GAMESS, and GAUSSIAN.

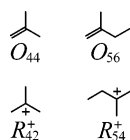
3.3.2. Evans–Polanyi Relationship. Whereas the single event concept accounts for the effect of the structure on the frequency factor of an elementary step, the Evans–Polanyi relationship¹⁶ accounts for the effect of structure and chain length upon the enthalpy contribution to the rate coefficient. For elementary steps belonging to a given type (methylation, β -scission, ...) the activation energy is related to the heat of reaction by

$$E_a(i) = E_a^\circ - \alpha |\Delta H_r(i)| \quad (\text{exothermic})$$

$$E_a(i) = E_a^\circ + (1 - \alpha) |\Delta H_r(i)| \quad (\text{endothermic}) \quad (9)$$

This relation permits the calculation of the activation

Chart 1



energy (E_a) for any elementary step or single event pertaining to a certain type, provided the α -coefficient and the E_a° of a reference step of that type are available. Use of modern quantum chemical packages, such as GAUSSIAN, is essential for the calculation of ΔH_f .

The single event rate coefficients can now be written:

$$\tilde{k} = \tilde{A} \exp\left(\frac{E_a}{RT}\right) \quad (10)$$

where \tilde{A} is the single event preexponential factor. The intrinsic activation barrier E_a° and the transfer coefficient α take on unique values for a given type of elementary step or single event so that there are only two independent rate parameters for this type of step. The single event concept and the Evans–Polanyi relation drastically reduce the number of rate coefficients.

3.4. Thermodynamic Constraints on the Parameters. Despite the remarkable reduction of the number of parameters in the rate expressions due to the introduction of the single event concept and the Evans–Polanyi relation, a large number of equilibrium constants still remains to be estimated. The number of these constants can also be reduced based upon thermodynamic relationships for the olefin isomerization network.

The equilibrium constant for the isomerization between any two olefins can be expressed as the product of the equilibrium constants for the reactions in their respective isomerization pathways via the common carbenium ions. Using this relation, together with the expression for the rate coefficient based upon the single event and the Evans–Polanyi relation, the protonation equilibrium constant for an olefin can be written as

$$K_{pr}(O_{ij}) = K_{Iso}(O_{ij}O_{ir})K_{pr}(O_{ir})\left(\frac{\sigma_{gl}^{R_{ir}^+}}{\sigma_{gl}^{R_{ij}^+}}\right) \times \exp\left(\frac{\Delta H_{f,g}(R_{ij}^+) - \Delta H_{f,g}(R_{ir}^+)}{RT}\right) \quad (11)$$

where O_{ir} and R_{ir}^+ represent the olefin and the corresponding carbenium ion in the reference protonation step. Olefins O_{44} and O_{56} (see Chart 1 for structures) are chosen as references for the olefins with carbon numbers 4 and 5, respectively. Similarly, carbenium ions R_{42}^+ and R_{54}^+ (see Chart 1 for structures) are chosen as references for the carbenium ions with carbon numbers 4 and 5, respectively.

Equation 11 shows that for olefins with the same carbon number, any protonation equilibrium constant can be calculated from the equilibrium constant of a reference protonation and the thermodynamic properties of the gas phase carbenium ions. Consequently, there is only one independent equilibrium constant per carbon number.

The use of the thermodynamic constraints, the single event kinetic approach, and the Evans–Polanyi relation for the energy contribution reduced the number of

parameters that need to be estimated to 30. Among these, 22 parameters relate to the formation of the primary olefins and eight relate to the higher olefins formation. These eight parameters are related to four heats of protonation of the reference olefins ($\Delta H_{pr}(O_{ir})$), one entropy term in the protonation equilibrium constant ($\Delta \tilde{S}_{pr}$), the single event frequency factor (\tilde{A}), the intrinsic activation barrier (E_a°), and the transfer coefficient (α). Because of the similarity between methylation and oligomerization, only one single event frequency factor for both types of elementary steps was considered.

To reduce the correlation between preexponential factors and activation energies and improve the significance of the estimated values, the rate coefficients were parametrized as follows: Starting from the Arrhenius form of the rate coefficient:

$$k_i = A \exp\left(-\frac{E_i}{RT}\right) \quad (12)$$

and after introduction of the mean temperature (T_m), the rate coefficients can be written as

$$k_i = \exp\left[\left(\ln A_i - \frac{E_i}{RT_m}\right) - \frac{E_i}{R}\left(\frac{1}{T} - \frac{1}{T_m}\right)\right] \quad (13)$$

The definition of the 30 parameters to be estimated is given in Table 4.⁸

4. Heats of Formation of Carbenium Ions

The heat of reaction of the elementary steps, required for the application of the Evans–Polanyi relation, is obtained from the heats of formation of olefins and surface-bonded carbenium ions. The thermodynamic properties of the olefin isomers are calculated using Benson's group contribution method; those of the surface associated carbenium ions were obtained in two steps. In the first, the properties of free carbenium ions were estimated by means of quantum chemical packages. The second step adds to these values the contributions arising from the link with the protons of the zeolite surface. The latter leads to a "heat of stabilization" that Park and Froment¹⁰ found to be a function of the number of C-atoms of the carbenium ions and is related to their heat of protonation. For lack of information in the literature, the latter were considered as parameters to be determined from the experimental data. Further details are provided by Park and Froment.¹⁰

5. Model Parameter Estimation

5.1. Experimental Data on SAPO-34. The experimental data used for the parameter estimation were obtained from Abraha.¹⁷ The experiments were conducted in a fixed bed reactor at three temperatures: 400, 425, and 450 °C. Catalyst powder was first pelletized by pressing it into wafers. These were then crushed and screened to 1.1 μm to avoid internal diffusion resistance. The catalyst bed was diluted 4 times (by weight) with α -alumina in three thin layers. Experiments at three different space times (g of catalyst/h/mol of methanol fed) were performed. The data were collected after 15 min, and it was assumed that at this time the catalyst did not contain any "coke" and had not deactivated yet. Varying the space time was achieved by changing the feed molar flow rate. The total pressure

Table 4. Parameters To Be Estimated⁸

P	definition	P	definition
1	$\frac{\Delta S_{\text{pr}}^{\circ}(\text{MeOH})}{R} - \frac{\Delta H_{\text{pr}}^{\circ}(\text{MeOH})}{RT_m}$	16	$\frac{E_{\text{sr}}(\text{OM};\text{H}^+)}{R}$
2	$\frac{\Delta H_{\text{pr}}^{\circ}(\text{MeOH})}{R}$	17	$\ln A_{\text{sr}}(\text{OM};\text{DMO}^+;\text{R}_2^+) - \frac{E_{\text{sr}}(\text{OM};\text{DMO}^+;\text{R}_2^+)}{RT_m}$
3	$\frac{\Delta S_{\text{hyd}}^{\circ}(\text{R}_1^+)}{R} - \frac{\Delta H_{\text{hyd}}^{\circ}(\text{R}_1^+)}{RT_m}$	18	$\frac{E_{\text{sr}}(\text{OM};\text{DMO}^+;\text{R}_2^+)}{R}$
4	$\frac{\Delta H_{\text{hyd}}^{\circ}(\text{R}_1^+)}{R}$	19	$\ln A_{\text{sr}}(\text{OM};\text{DMO}^+;\text{R}_3^+) - \frac{E_{\text{sr}}(\text{OM};\text{DMO}^+;\text{R}_3^+)}{RT_m}$
5	$\ln A_{\text{c}}(\text{R}_1^+) - \frac{E_{\text{c}}(\text{R}_1^+)}{RT_m}$	20	$\frac{E_{\text{sr}}(\text{OM};\text{DMO}^+;\text{R}_3^+)}{R}$
6	$\frac{E_{\text{c}}(\text{R}_1^+)}{R}$	21	$\ln A_{\text{pr}}(\text{O}_2) - \frac{E_{\text{pr}}(\text{O}_2)}{RT_m}$
7	$\ln A_{\text{F}}(\text{DME}) - \frac{E_{\text{F}}(\text{DME})}{RT_m}$	22	$\frac{E_{\text{pr}}(\text{O}_2)}{R}$
8	$\frac{E_{\text{F}}(\text{DME})}{R}$	23	$\frac{\Delta \tilde{S}_{\text{pr}}}{R}$
9	$\frac{\Delta S_{\text{pr}}^{\circ}(\text{DME})}{R} - \frac{\Delta H_{\text{pr}}^{\circ}(\text{DME})}{RT_m}$	24	$\frac{\Delta H_{\text{pr}}^{\circ}(\text{O}_2)}{R}$
10	$\frac{\Delta H_{\text{pr}}^{\circ}(\text{DME})}{R}$	25	$\frac{\Delta H_{\text{pr}}^{\circ}(\text{O}_3)}{R}$
11	$\ln A_{\text{F}}(\text{CH}_4) - \frac{E_{\text{F}}(\text{CH}_4)}{RT_m}$	26	$\frac{\Delta H_{\text{pr}}^{\circ}(\text{O}_{4r})}{R}$
12	$\frac{E_{\text{F}}(\text{CH}_4)}{R}$	27	$\frac{\Delta H_{\text{pr}}^{\circ}(\text{O}_{5r})}{R}$
13	$\ln A_{\text{sr}}(\text{R}_1^+;\text{bs}) - \frac{E_{\text{sr}}(\text{R}_1^+;\text{bs})}{RT_m}$	28	$\ln(C_{\text{H}^+}^{\dagger} \cdot \bar{A})$
14	$\frac{E_{\text{sr}}(\text{R}_1^+;\text{bs})}{R}$	29	α
15	$\ln A_{\text{sr}}(\text{OM};\text{H}^+) - \frac{E_{\text{sr}}(\text{OM};\text{H}^+)}{RT_m}$	30	$\frac{E^{\circ}}{R\alpha}$

inside the reactor was 1.04 bar for all the experiments. To decrease the deactivation rate of SAPO-34, all the experiments were conducted with 80 mol % water in the feed. The experimental data used in the present work are shown in Figure 3. Both ethylene and propylene are produced in almost equal quantities, but the temperature affects the ratio to some extent.

Assuming plug flow in the experimental reactor the predicted responses (\hat{y}_i) are calculated from the following continuity equations:

$$\frac{d\hat{y}_i}{d(W/F_{\text{MeOH}}^{\circ})} = \frac{100M_i}{M_{\text{MeOH}}}\mathcal{R}_i \quad i = 1, 2, \dots, m \quad (14)$$

This set of stiff differential equations can be solved numerically using Gear's method and with the initial condition of zero yields at zero space time.

5.2. Physicochemical Constraints. Because the rate parameters defined above are fundamental they should satisfy well-established physicochemical laws.

Boudart's criteria¹⁸ define a rigorous set of constraints for the enthalpies and entropies:

$$-\Delta H_{\text{pr}}^{\circ} > 0$$

$$0 < -\Delta S_{\text{pr}}^{\circ} < S_{\text{g}}^{\circ}$$

$$41.8 < -\Delta S_{\text{pr}}^{\circ} < 51.04 + 1.4 \times 10^{-3}(-\Delta H_{\text{pr}}^{\circ}) \quad (15)$$

where S_{g}° is the standard entropy of the molecule in the gas phase. To ensure that the estimated parameters have meaningful values, the above criteria were inserted as constraints into the optimization routine.

5.3. Estimation Procedure. The estimation of the kinetic parameters was based upon the minimization of the difference between the experimental and calculated methanol conversion and yields of MTO products:

$$S = \sum_{j=1}^m \sum_{l=1}^m w_{jl} \sum_{i=1}^n (y_{ij} - \hat{y}_{ij})(y_{il} - \hat{y}_{il}) \quad (16)$$

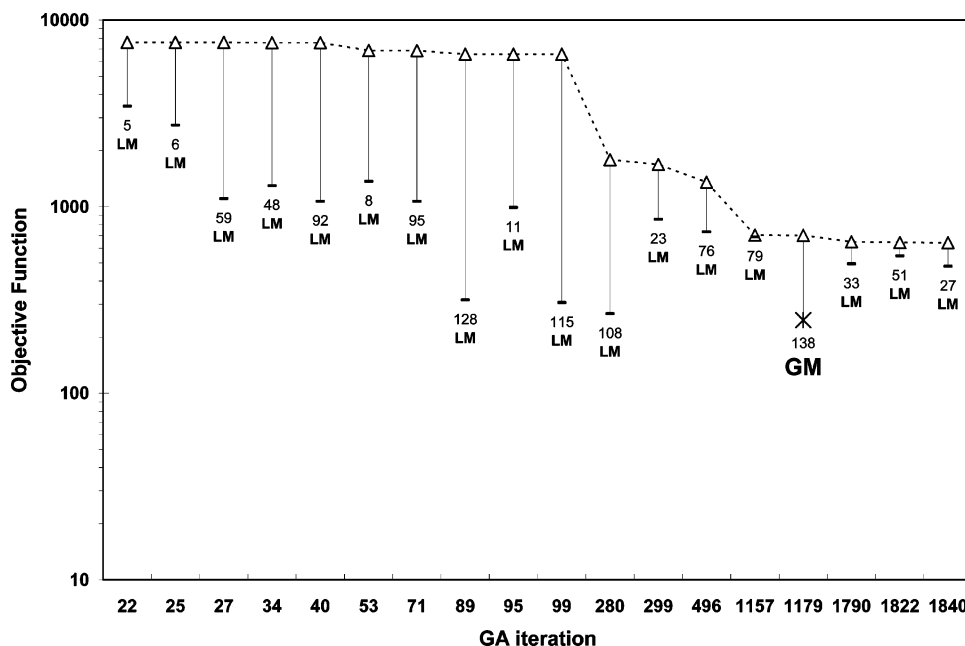


Figure 2. Estimation of the kinetic parameters for MTO on SAPO-34 by the hybrid genetic algorithm. ($\cdots\Delta\cdots$) Objective function after each GA iteration. (—) Minimization by the Levenberg–Marquardt optimizer. LM, local minimum; GM, global minimum.

where m = number of responses, n = number of experiments, and w_{jl} = elements of the inverse of the covariance matrix of the experimental errors on the responses y .

The minimization of the objective function S was based upon the Hybrid Genetic Algorithm developed by Park and Froment.¹⁹ In this algorithm, three different routines are combined with the objective of increasing the efficiency and the accuracy of the estimation procedure. In the beginning, the Genetic Algorithm is used to generate the initial guesses for the local optimizer. A constrained optimization technique based upon sequential quadratic programming, called FFSQP, was used for this to ensure that all the estimated parameters satisfied the constraints discussed before. The minimization of the objective function by FFSQP was checked and eventually pursued by an unconstrained Levenberg–Marquardt package, also performing statistical tests and determining confidence intervals for the parameters. To guarantee that the best set arrived at by means of the Levenberg–Marquardt technique still satisfied the constraints, an ultimate loop through GA and FFSQP was inserted into the procedure.

Figure 2 shows the minimization progress performed by the Hybrid Genetic Algorithm. The best sets of parameters generated by the GA were used as starting point for the Levenberg–Marquardt and Quadratic Sequential Programming (FFSQP) optimizers. The global minimum (GM) was reached after performing 138 iterations with the latter two optimizers, starting from the set of parameter values reached after 1179 GA iterations and corresponding to a value of the objective function of the order of 800.

5.4. Parameter Values and Comparison of Experimental and Calculated Yields. The parameters estimated by the hybrid GA are shown in Table 5, along with their approximate 95% confidence interval. The first column represents the parameters obtained after parametrization of the rate and equilibrium constants, as listed in Table 4. Kinetic parameters were derived from these values using the total concentration of the acid and basic sites. Because of the similarity between

methylation and oligomerization only one single event frequency factor was considered for both types of elementary steps. All the parameters satisfy the statistical tests and—by the very nature of the estimation procedure—the physicochemical constraints. The low value of the transfer coefficient could be an indication, according to Hammond's postulate,²⁰ that the structure of the activated complex is close to that of the reactant. A slightly larger value of α was obtained for ZSM-5 ($\text{Si}/\text{Al} = 200$).⁸ The heat of protonation of the reference olefins levels off from propylene onward for SAPO-34, whereas a slight decrease of ΔH_{pr} was observed for ZSM-5. The single event frequency factor of methylation and oligomerization on ZSM-5 is around 25 times larger than that obtained on SAPO-34.

The kinetic model based on the estimated parameters leads to an excellent fit of the experimental data. The fit of the experimental methanol conversion and of the various product yields as a function of space time is shown, by way of example, for 450 °C in Figure 3. The kinetic model also reproduced the experimental data of Marchi and Froment,²¹ also obtained on SAPO-34, as shown in Table 6.

6. Single Event Rate Coefficients for the Various Elementary Steps

The parameter values of Table 5 now enable the calculation of the single event rate coefficients. The single event frequency factor (\bar{A}) for a given type of elementary step is independent of the structure. Because of the energetics, however, that does not necessarily mean that the single event rate coefficient (\bar{k}) is also independent of the structure.

Figure 4 shows the effect of chain length on the single event rate coefficients for the methylation of linear olefins and for their oligomerization by means of the ethyl- R^+ at 440 °C. The produced carbenium ions are all linear and secondary. The single event rate coefficient significantly increases with chain length. Since, by virtue of the single event concept, there is only one frequency factor in this model, this effect solely results

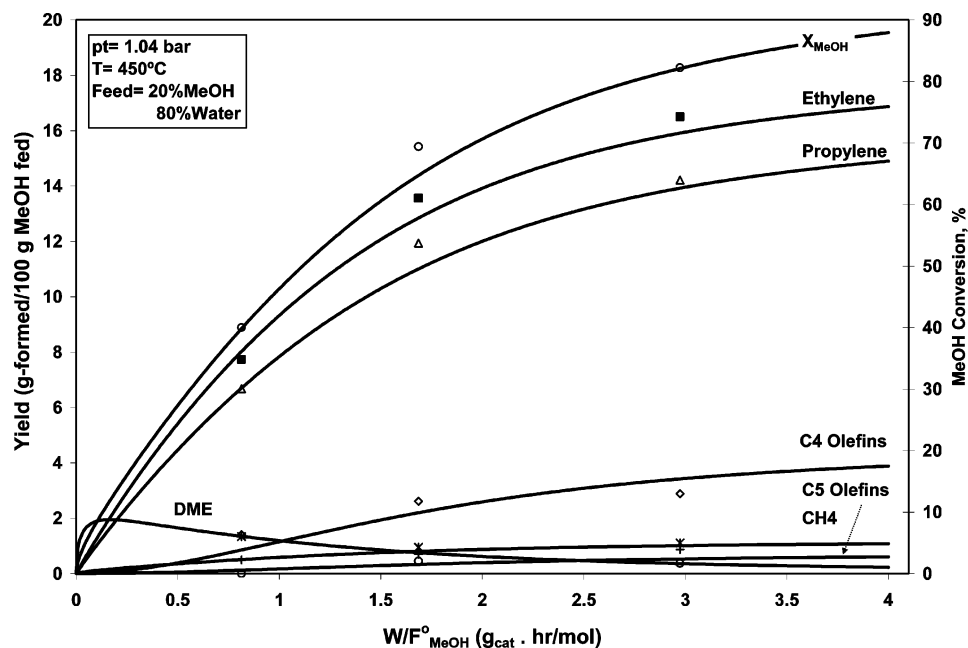


Figure 3. Comparison of calculated and experimental yields of various MTO products on SAPO-34. Lines, simulation; symbols, experimental.

Table 5. Value of the Kinetic Parameters for MTO on SAPO-34

P	P estimate	95% confidence interval		derived kinetic parameters	values	units
		lower	upper			
1	1.818E-01	1.555E-01	2.081E-01	$\Delta S_{pr}(\text{MeOH})$	-1.22E+02	$\text{J}\cdot\text{mol}^{-1}\cdot\text{K}^{-1}$
2	-1.055E+04	-1.092E+04	-1.017E+04	$\Delta H_{pr}(\text{MeOH})$	-8.77E+01	$\text{KJ}\cdot\text{mol}^{-1}$
3	-2.726E+00	-3.009E+00	-2.443E+00	$\Delta S_{hyd}(\text{R}_1^+)$	-3.32E+01	$\text{J}\cdot\text{mol}^{-1}\cdot\text{K}^{-1}$
4	-9.009E+02	-9.104E+02	-8.914E+02	$\Delta H_{hyd}(\text{R}_1^+)$	-7.49E+00	$\text{KJ}\cdot\text{mol}^{-1}$
5	6.339E+00	5.715E+00	6.963E+00	$A'_C(\text{R}_1^+)$	1.05E+02	$\text{s}^{-1}\cdot\text{bar}^{-1}$
6	1.224E+02	1.128E+02	1.318E+02	$E_C(\text{R}_1^+)$	1.02E+00	$\text{KJ}\cdot\text{mol}^{-1}$
7	5.121E+00	4.850E+00	5.392E+00	$A'_F(\text{DME})$	3.09E+01	$\text{s}^{-1}\cdot\text{bar}^{-1}$
8	1.200E+02	1.143E+02	1.257E+02	$E_F(\text{DME})$	9.98E-01	$\text{KJ}\cdot\text{mol}^{-1}$
9	1.155E+01	9.394E+00	1.372E+01	$\Delta S_{pr}(\text{DME})$	-4.18E+01	$\text{J}\cdot\text{mol}^{-1}\cdot\text{K}^{-1}$
10	-1.183E+04	-1.197E+04	-1.168E+04	$\Delta H_{pr}(\text{DME})$	-9.83E+01	$\text{KJ}\cdot\text{mol}^{-1}$
11	2.016E+00	1.766E+00	2.267E+00	$A'_C(\text{CH}_4)$	1.00E+13	$\text{s}^{-1}\cdot\text{bar}^{-1}$
12	2.123E+04	2.096E+04	2.150E+04	$E_F(\text{CH}_4)$	1.77E+02	$\text{KJ}\cdot\text{mol}^{-1}$
13	5.694E+00	5.521E+00	5.867E+00	$A'_{sr}(\text{R}_1^+;\text{bs})$	1.67E+16	s^{-1}
14	2.136E+04	2.105E+04	2.167E+04	$E_{sr}(\text{R}_1^+;\text{bs})$	1.78E+02	$\text{KJ}\cdot\text{mol}^{-1}$
15	1.374E+01	1.239E+01	1.510E+01	$A'_{sr}(\text{OM};\text{H}^+)$	1.97E+17	s^{-1}
16	1.738E+04	1.717E+04	1.758E+04	$E_{sr}(\text{OM};\text{H}^+)$	1.45E+02	$\text{KJ}\cdot\text{mol}^{-1}$
17	5.192E+00	5.069E+00	5.315E+00	$A'_{sr}(\text{OM};\text{DMO}^+;\text{R}_2^+)$	2.03E+05	s^{-1}
18	3.798E+03	3.777E+03	3.819E+03	$E_{sr}(\text{OM};\text{DMO}^+;\text{R}_2^+)$	3.16E+01	$\text{KJ}\cdot\text{mol}^{-1}$
19	4.613E+00	4.434E+00	4.793E+00	$A'_{sr}(\text{OM};\text{DMO}^+;\text{R}_3^+)$	2.29E+03	s^{-1}
20	1.013E+03	9.575E+02	1.069E+03	$E_{sr}(\text{OM};\text{DMO}^+;\text{R}_3^+)$	8.43E+00	$\text{KJ}\cdot\text{mol}^{-1}$
21	-3.560E+00	-3.759E+00	-3.361E+00	$A'_{pr}(\text{O}_2)$	7.64E+03	$\text{s}^{-1}\cdot\text{bar}^{-1}$
22	1.024E+04	1.014E+04	1.033E+04	$E_{pr}(\text{O}_2)$	8.51E+01	$\text{KJ}\cdot\text{mol}^{-1}$
23	-1.292E+01	-1.371E+01	-1.213E+01	ΔS_{pr}	-1.08E+02	$\text{J}\cdot\text{mol}^{-1}\cdot\text{K}^{-1}$
24	-6.741E+03	-6.777E+03	-6.705E+03	$\Delta H_{pr}(\text{O}_2)$	-5.61E+01	$\text{KJ}\cdot\text{mol}^{-1}$
25	-1.200E+04	-1.205E+04	-1.196E+04	$\Delta H_{pr}(\text{O}_3)$	-9.98E+01	$\text{KJ}\cdot\text{mol}^{-1}$
26	-1.200E+04	-1.215E+04	-1.186E+04	$\Delta H_{pr}(\text{O}_{4r})$	-9.98E+01	$\text{KJ}\cdot\text{mol}^{-1}$
27	-1.200E+04	-1.205E+04	-1.196E+04	$\Delta H_{pr}(\text{O}_{5r})$	-9.98E+01	$\text{KJ}\cdot\text{mol}^{-1}$
28	1.520E+01	1.459E+01	1.581E+01	\bar{A}'	6.27E+05	$\text{s}^{-1}\cdot\text{bar}^{-1}$
29	1.647E-02	1.041E-02	2.254E-02	α	1.65E-02	dimensionless
30	7.067E+05	6.996E+05	7.137E+05	E^o	9.68E+01	$\text{KJ}\cdot\text{mol}^{-1}$

from the enthalpy contribution to the single event rate coefficient. It should be noted here that the Figure 4, like the following Figures 5–7, also deals with species having carbon numbers beyond those reported in Figure 3. These species are actually formed inside the SAPO-34 cavities but cannot exit them. They are included here for the sake of illustrating the effect of structures and properties of carbenium ions and olefins on the values of the single event rate coefficient.

Figure 5 illustrates the effect of branching, expressed in terms of $n_{C\alpha-C}$ (number of carbon atom in α position with respect to the carbon carrying the positive charge) in the produced R^+ and of the nature of R^+ on the k for methylation. A comparison of curve a and curve b (corresponding to R^+), which are respectively all tertiary and all secondary, reveals that the effect of the nature of R^+ is far more pronounced than that of branching.

Table 6. Model Verification by Comparison with Experimental Data of Marchi and Froment²¹ Obtained under Entirely Different Space Time^a

	yield model	(wt %) expt
ethylene	13.7	14.2
propylene	11.7	13.0
C ₄ olefins	7.9	5.4
C ₅ olefins	1.8	1.3
methane	3.1	2.7
DME	0	0
methanol conversion (%)	100	100

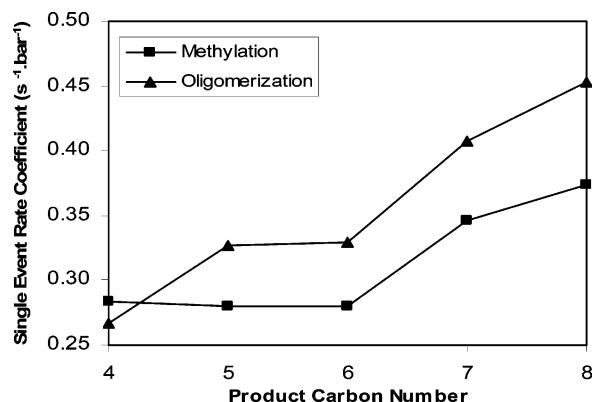
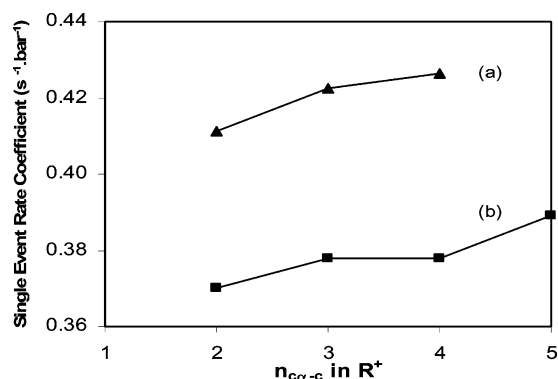
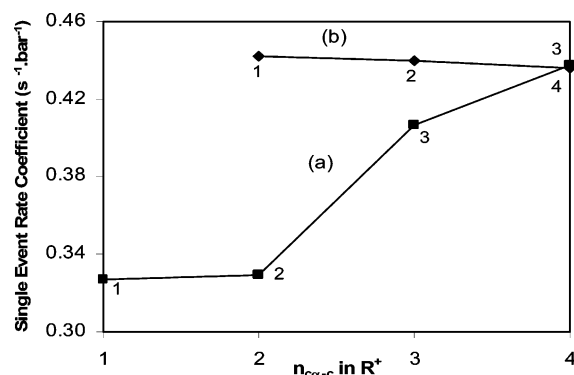
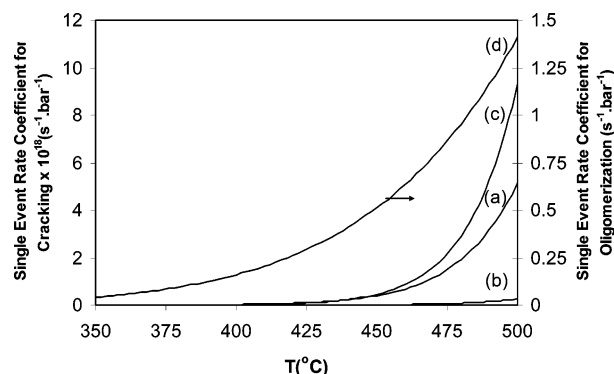
^a Temperature: 480 °C. Pressure: 1.04 bar.**Figure 4.** Single event rate coefficients for the methylation and oligomerization of linear olefins as a function of the C-number of the product.**Figure 5.** Single event methylation rate coefficients. Effect of structure of reacting olefin. Curve a: all C7 olefins. Produced R^+ : 2,3-diMe-2-hexyl; 2,5-diMe-3-hexyl; 2,3,4-triMe-3-pentyl. Curve b: all C7 olefins. Produced R^+ : 2-Me-3-heptyl; 4-Me-3-heptyl; 3,3-diMe-4-hexyl; 2,2,4-triMe-3-pentyl.

Figure 6 deals with oligomerization by means of the ethyl- R^+ . All the produced carbenium ions are secondary. Curve a shows how \bar{k} increases with chain length and/or $n_{C\alpha-C}$. From curve b, corresponding to C₆ olefins, branched or straight, it follows that the effect of branching is very weak.

Figure 7 shows the evolution with temperature of the single event rate coefficient of the β -scission of various octyl- R^+ . The \bar{k} values are seen to take off from 460 °C onward. A similar behavior is observed for the evolution with temperature of oligomerization \bar{k} (curve d), which is the reverse of the β -scission in curve b. These trends are all in line with those observed for MTO on ZSM-5.

7. Effect of Operating Conditions on the Ethylene and Propylene Yields

The kinetic model is an outstanding tool for the exploration of the effect of process variables on the yields

**Figure 6.** Single event oligomerization rate coefficients. Carbenium ion: ethyl. Effect of olefin structure. Curve a: (1) propylene; (2) 1-butene; (3) 2-Me-2-butene; (4) 2-Me-3-pentene. Curve b: (1) 2-Me-4-pentene; (2) 2-hexene; (3) 2-Me-3-pentene.**Figure 7.** Single event rate coefficients for elementary cracking steps. Curve a: 2,2-diMe-4-hexyl R^+ into 1-butene and 2-Me-2-propyl R^+ . Curve b: 2,2,4-triMe-4-pentyl R^+ into isobutylene and 2-Me-2-propyl R^+ . Curve c: 3,4-diMe-5-hexyl R^+ into 2-butene and 2-butyl R^+ . Curve d: Single event rate coefficient for the oligomerization step that is the reverse of the cracking step of curve b.

of the various products. Figures 8 and 9 summarize the results of simulations of the process in an isothermal plug flow reactor.

Figure 8 shows that the temperature strongly affects the ratio of ethylene to propylene yields. The maximum propylene yield of 12.7 wt % is obtained around 425 °C, but from there on it drops below the ethylene yield, which monotonically increases. The ethylene/propylene ratio continuously increases with temperature from a value of 0.6 at 375 °C to 1.2 at 475 °C. For all cases, the exit conversion of methanol was kept constant at 85%, and the feed did not contain any water.

Figure 9 shows that for a methanol conversion of 85% and a temperature of 450 °C water addition favors both the ethylene and propylene yields, but the effect on their ratio is very weak, in agreement with experimental results shown in Table 7 of the review of Froment et al.²

8. Catalyst Deactivation

8.1. Introduction. As discussed earlier, SAPO-34 suffers relatively rapid deactivation in MTO. The rapid deactivation was attributed to both coverage of the acid sites and blockage of pore structure.² Figure 10 shows a typical deactivation behavior of a SAPO-34 catalyst, as measured by Froment et al.² M is defined as the total weight of methanol fed to the reactor during the run per unit weight of catalyst.

Figure 10 shows that the yield of C₂–C₄ olefins does not decline immediately and that the DME yield rises

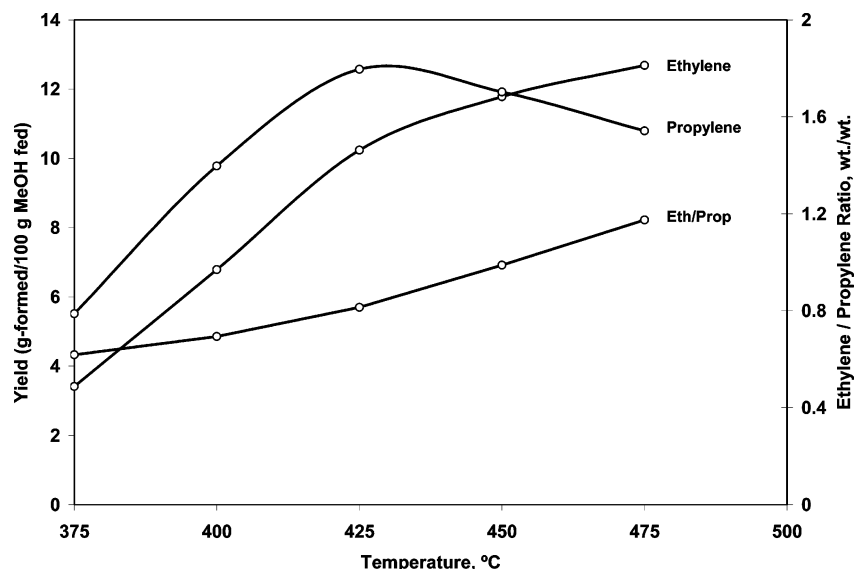


Figure 8. Effect of temperature on ethylene and propylene yields at a methanol conversion of 85%. No water in the feed.

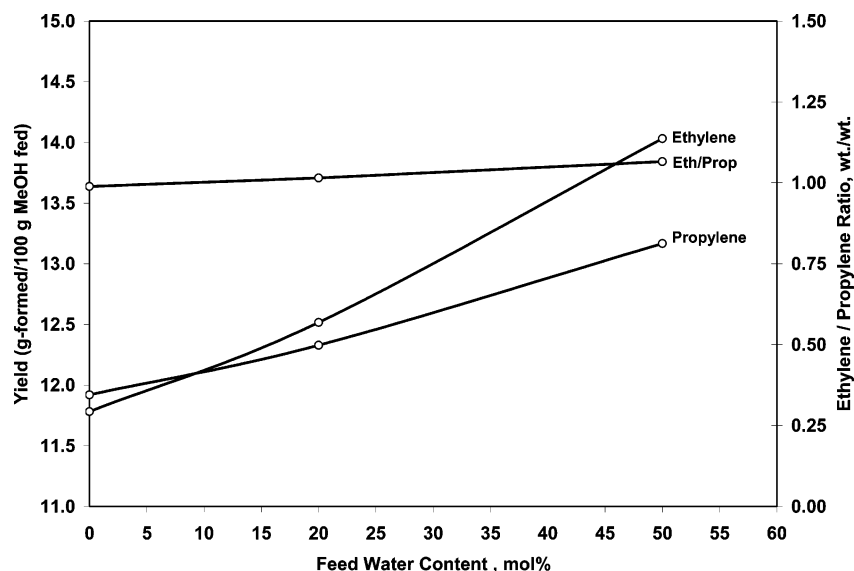


Figure 9. Effect of water content of the feed on ethylene and propylene yields for a methanol conversion of 85% and a temperature of 450 °C.

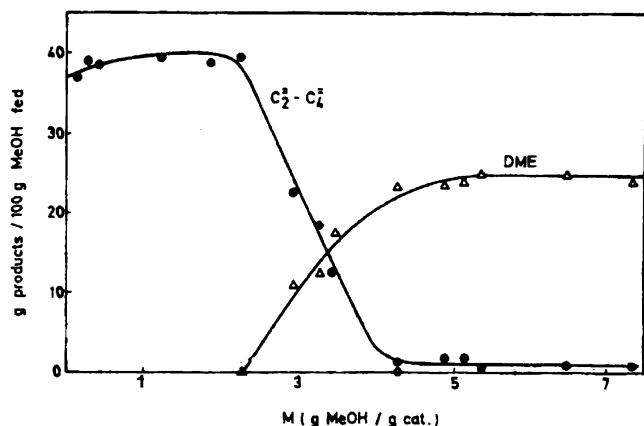


Figure 10. Methanol conversion into hydrocarbons on SAPO-34. $T = 480$ °C; feed 20/80 mol % methanol–water. $M = \Sigma F_{\text{MeOH}}/W$. Yields of C_2 – C_4 olefins and DME.²

only from a certain M -value onward. This does not mean that the catalyst deactivation does not start right away as feed is being introduced into the reactor, however. The delay is a consequence of the high rate of the MTO

reactions, causing the process to occur initially in a thin slice of the catalyst bed. As the catalyst deactivates the slice broadens. Only after it has spread through the entire bed, the deactivation is observed at the reactor exit.

Figure 10 also reveals that for longer process times the olefin yield drops to zero, while the DME yield, after increasing from zero to 30%, becomes constant. This illustrates that the conversion of methanol into DME does not deactivate to the same extent as that into hydrocarbons. The direct implication is that different deactivation functions are required for the methanol conversion and for the yields of olefins. That for the olefins is exponential and drops to zero, that for the methanol conversion into DME is a hyperbolic function, not dropping to zero. In this work, the deactivation of SAPO-34 is modeled based upon the single event concept and then introduced into the kinetic equations for the purpose of simulating the reactor behavior.

8.2. Modeling of Catalyst Deactivation. The deactivation is ascribed to higher oligomerization products (C_6 – C_8) which, because of the cavity structure of SAPO-

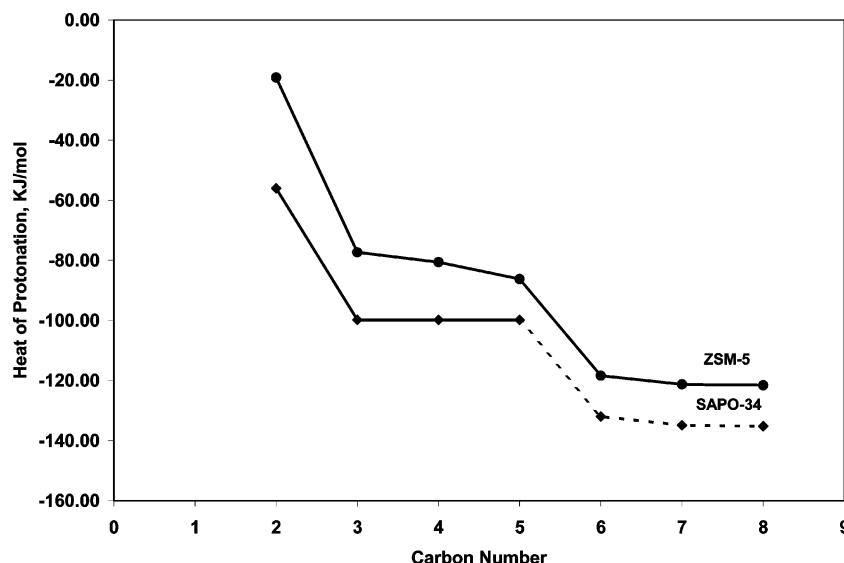


Figure 11. Extrapolation of heats of protonation of C_{6+} olefins on SAPO-34 based upon corresponding values for ZSM-5. Solid line: estimated from experiments; broken line: extrapolated.

34, cannot leave the catalyst. They permanently cover the acid active sites and/or block pores, thus causing deactivation of the catalyst and a decline of the methanol conversion and yields of the various products. The C_{6+} products cannot be observed at the exit of the reactor, but their rate of formation and concentration inside the cages can be calculated making use of the single event concept in the following way.

Because the single event frequency factor for methylation and oligomerization is independent of structure and chain length of the species, the frequency factor calculated for the steps involved in the formation of C_4 and C_5 olefins can be used to calculate the rate of formation of the C_{6+} components. The activation energies of C_{6+} formation and cracking can be calculated from the Evans–Polanyi relationship given the heat of reaction of the elementary step. The latter is calculated from the heats of formation of the reactant and the activated complex. These are obtained from ab initio quantum chemical calculations.

The heats of protonation of reference olefins ($\Delta H_{pr}(O_{ir})$) for carbon numbers up to C_5 are estimated from experimental data, as discussed before. The heats of protonation for C_{6+} olefins are not known for SAPO-34 however. To calculate them, it is assumed that the heats of protonation for the reference olefins with different carbon number have the same trend for SAPO-34 as for ZSM-5. This assumption is verified by comparing the values of $\Delta H_{pr}(O_{ir})$ obtained for SAPO-34 up to C_5 olefins with those of ZSM-5, estimated by Park and Froment,⁸ as shown in Figure 11. The heats of protonation of the C_{6+} reference olefins are obtained by extrapolation.

At any point along the plug flow reactor the concentration of the C_{6+} components evolves with time according to

$$\frac{\partial C_{C_{6+}}}{\partial t} = \Phi_c r_c \quad (17)$$

with initial condition

$$\text{at } t = 0, C_{C_{6+}} = 0 \text{ for all } \frac{W}{F_{MeOH}}$$

where

$$r_c = \sum_6^8 M_i \mathcal{R}_i$$

Φ_c is the deactivation function for C_{6+} olefins formation. It is expressed in terms of the concentration of the C_{6+} olefins using the well-proven empirical correlation proposed by Froment and Bischoff²² as

$$\Phi_c = \exp(-\alpha C_{C_{6+}})$$

Equation 17 has to be integrated simultaneously with the set of continuity equations describing the behavior of methanol and the various reaction products in the reactor:

$$\frac{\partial \dot{Y}_i}{\partial (W/F_{MeOH})} = \frac{100 M_i}{M_{MeOH}} \Phi_i \mathcal{R}_i \quad i = 1, 2, \dots, m \quad (18)$$

where Φ_j are deactivation functions, expressed as follows:

$$\Phi = \exp(-\alpha C_{C_{6+}}) \quad \text{for olefins formation} \quad (19)$$

$$\Phi = \frac{1}{(1 + \beta C_{C_{6+}})} \quad \text{for methanol conversion} \quad (20)$$

Equations 17–20 contain two unknown parameters (α and β) that need to be estimated. The experimental data of Marchi and Froment²¹ were utilized for this purpose. The parameters were estimated by minimizing the difference between the experimental and the calculated methanol conversions and C_2 – C_4 yields. Calculated values are obtained by solving the system of partial differential eqs 17–20.

First, Gear's method was used to integrate eq 19 along the length of the reactor. Once the yields for different products are calculated at zero time, eq 17 was integrated with respect to time, thus leading to the C_{6+} concentration for the next time increment along the length of the reactor. The Runge–Kutta method was used for time integration. Because Gear's method uses

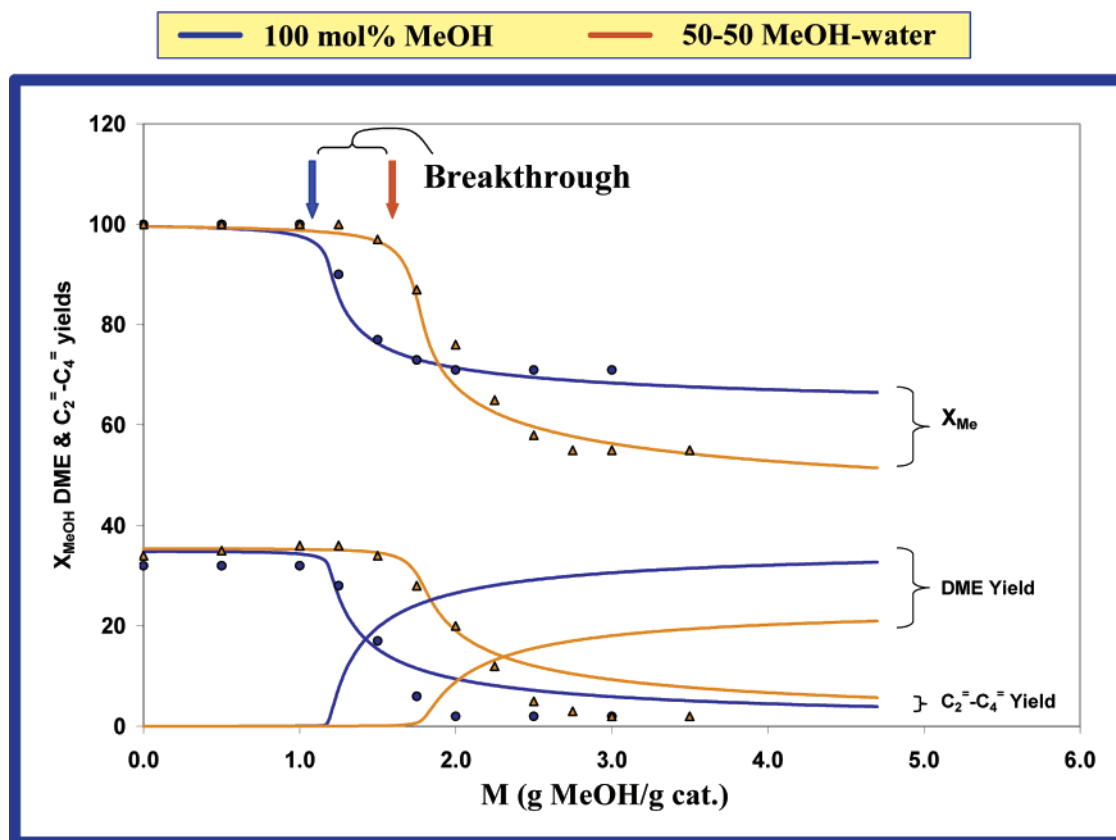


Figure 12. Fitting of the experimental data of Marchi and Froment obtained in an isothermal fixed bed reactor at 480 °C, 1.04 bar total pressure, $W/F_{\text{MeOH}}^0 = 32.0$, and for a methanol partial pressures of 1.04 (circles) and 0.52 bar (triangles). Points: experimental data; lines: simulated.

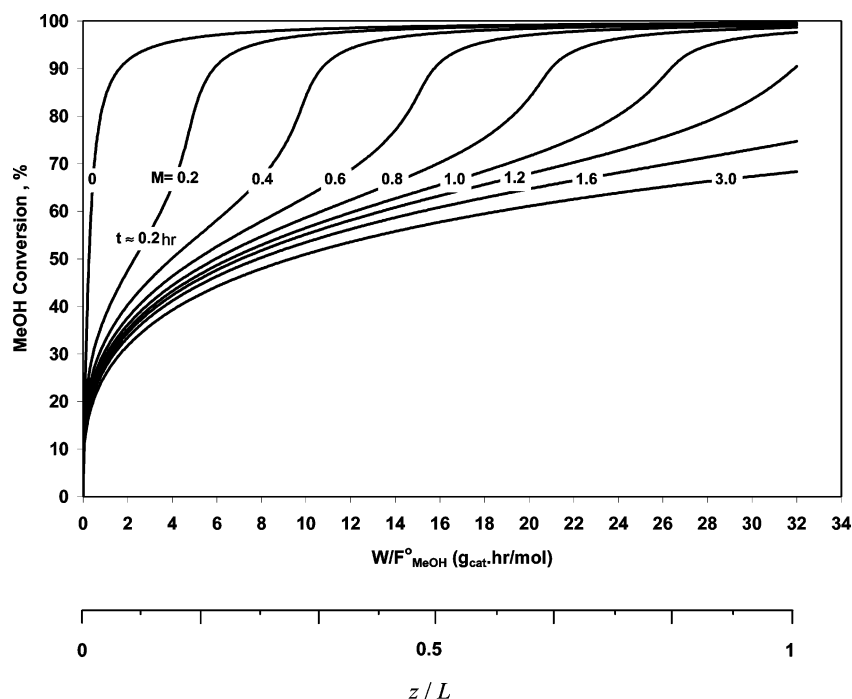


Figure 13. Simulated profiles of methanol conversion at different process times for an isothermal fixed bed reactor at 480 °C, 1.04 bar total pressure, and pure methanol feed.

a variable step size, interpolation between known C_{6+} concentration values are needed to calculate the values at any space time. At this point product yields are calculated based on the new C_{6+} concentration profiles. This mathematical loop is continued until the final process time is reached.

8.3. Results and Discussion. An accurate fit of the experimental data of Marchi and Froment²¹ required deactivation constants depending upon the partial pressure of methanol in the feed (i.e., on the water dilution). For a methanol partial pressure in the feed of 1.04 bar (no water), α amounted to 60 and β amounted to 7.5.

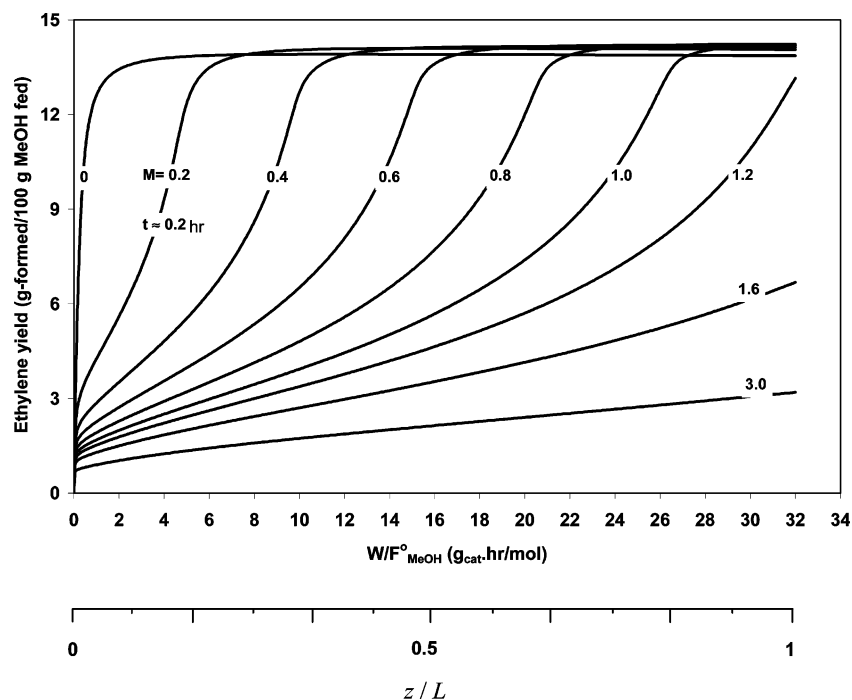


Figure 14. Evolution of ethylene yield profiles with total amount of methanol fed per unit amount of catalyst or process time in an isothermal fixed bed reactor at 480 °C, 1.04 bar total pressure, and pure methanol feed.

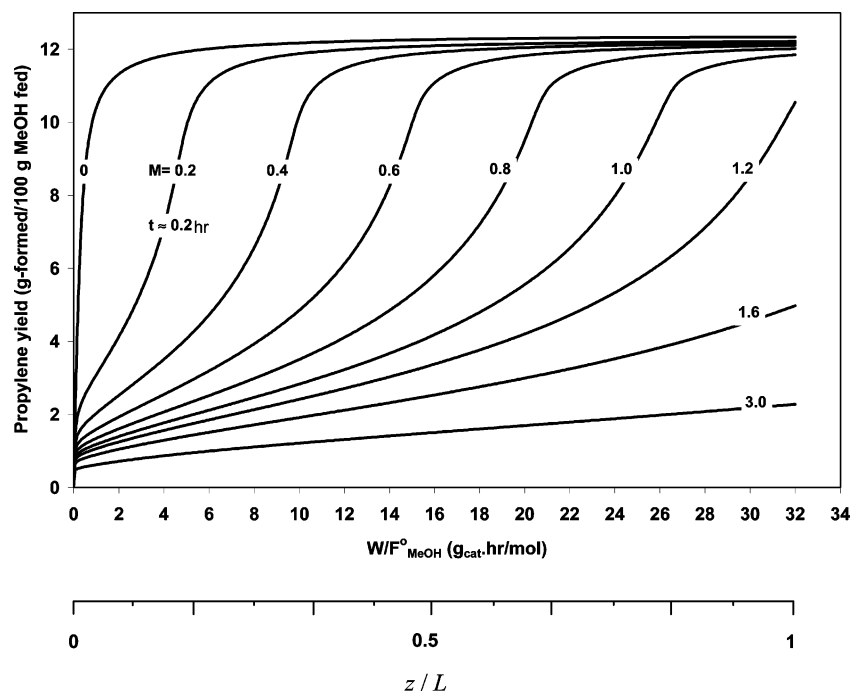


Figure 15. Evolution of the propylene yield profiles with process times or total amount of methanol fed per unit catalyst weight for an isothermal fixed bed reactor at 480 °C, 1.04 bar total pressure, and fed with methanol only.

For a methanol partial pressure of 0.52, the corresponding values were 80 and 46, reflecting slower deactivation in the presence of water. The rate coefficients are those calculated from the parameters given in Table 5.

Figure 12 compares the methanol conversion and C₂–C₄ olefins yield predicted by the model with the experimental data of Marchi and Froment²¹ performed at 480 °C, 1.04 bar total pressure, and partial pressures of methanol of 1.04 and 0.52. The data are plotted versus the total amount of methanol fed per gram catalyst, which is proportional to the run length or process time.

The matching between the model and the experimental data is very good, except for the very low C₂–C₄ olefins yield observed for long run lengths and which are slightly overpredicted. Experimental data for the DME yield are not available for these conditions.

It follows from Figure 12 that the MeOH conversion does not drop instantaneously after the start of the operation but instead remains constant for some time. This does not mean that the catalyst is not deactivating during that period, however. The breakthrough point depends on the amount of catalyst and the water content of the feed. The higher the water content in the

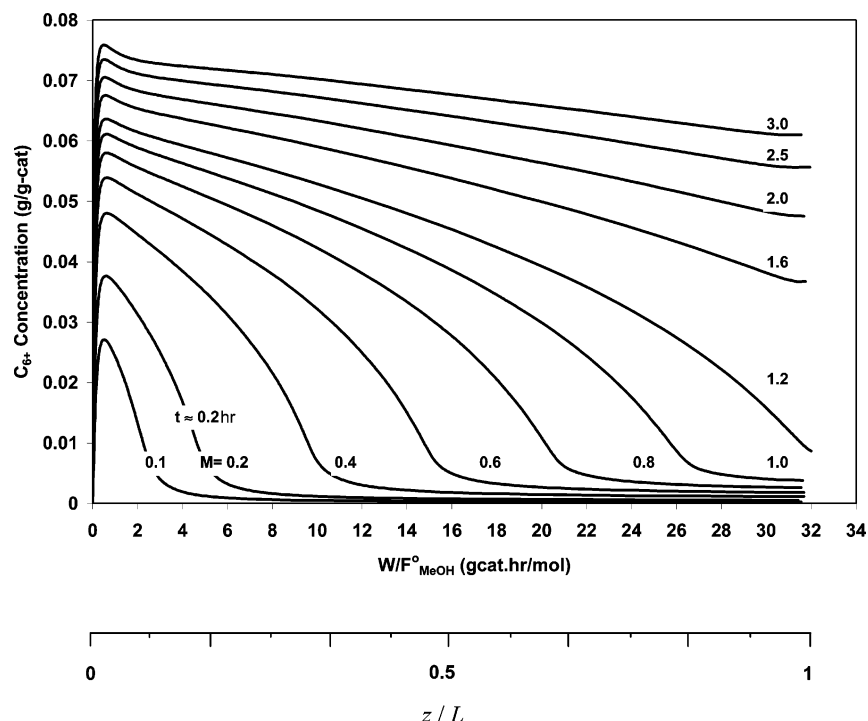


Figure 16. Concentration profiles of C_{6+} olefins inside the catalyst at various process times for isothermal fixed bed reactor at 480 °C, 1.04 bar total pressure, and pure methanol feed.

feed, the longer the conversion stays unaffected. The total conversion of methanol drops to 70% for pure methanol feed. That could correspond to equilibrium with DME, which is not felt for short process times because DME is continuously converted into olefins, without strong effect of deactivation yet.

Figures 13–15 show the evolution of the methanol conversion, of the ethylene and propylene yields in the reactor at various M or process times, and for a 100% methanol feed. The figures further explain the behavior of the MeOH conversion inside the reactor in the presence of deactivation. The deactivation is not observed at the exit of the reactor until the breakthrough point is reached.

Figure 16 shows that the concentration of the C_{6+} olefins, which are trapped inside the SAPO-34 cavities, reaches a maximum near the inlet of the reactor. This behavior can be explained by rapid production and simultaneous decomposition by β -scission. The cracking of the C_{6+} olefins into smaller olefins is fast for short process times, but as time increases the cracking slows down due to deactivation.

Additional simulations showed that it is possible to decrease the formation of C_{6+} component and thus slow the deactivation of the catalyst by increasing the partial pressure of water in the feed. This effect of water was indeed previously observed for SAPO-34.²¹ When water was replaced by nitrogen, the deactivation was not reduced.

9. Conclusion

The kinetics of MTO on SAPO-34 were modeled in terms of the fundamental single event approach and the effect of the structure of reactants and products on the single event kinetic parameters was analyzed. The results are completely in line with previous results obtained with ZSM-5, except that, because of the structure of SAPO-34, hydrocarbons with 6 or more

C-atoms are not detected in the exit product. These components are withheld inside the cavities and cause deactivation. The latter becomes obvious only after the reactions have slowed sufficiently to spread out over the complete catalyst bed, instead of occurring in a small zone near the inlet. The single event approach allowed to model the deactivation in terms of the amount of C_{6+} olefins produced. Specific aspects of the behavior of MTO on SAPO-34 were then illustrated by the simulation of an isothermal fixed bed reactor.

Acknowledgment

The authors are grateful to Dr. R. G. Anthony (Texas A&M University) and to Dr. T.-Y. Park (SABIC Technology Center, Houston, TX) for stimulating discussions.

Nomenclature

- A' = preexponential factor of an elementary step
- \bar{A} = single event preexponential factor
- C_{bs}^t = total concentration of basic sites (kmol/kg of catalyst)
- $C_{H^+}^t$ = total concentration of acidic sites (kmol/kg of catalyst)
- $C_{C_{6+}}$ = weight content of C_{6+} olefins inside the catalyst (kg/kg of catalyst)
- E_a^o = intrinsic activation barrier in Evans–Polanyi relation (kJ/kmol)
- F_{MeOH}^o = initial flow rate of methanol at inlet of reactor (kmol/h)
- h = Plank constant: 1.841×10^{-37} (J h)
- K_i = equilibrium constant for elementary step i
- k_B = Boltzmann constant: 1.381×10^{-23} (J/K)
- k_i = rate coefficient for elementary step i
- $k_i'(j,k)$ = rate coefficient for elementary step of type i at j th category and k th reaction
- \bar{k} = single event rate coefficient
- M_j = molecular weight of species j (kg/kmol)
- m = mass flow rate (kg/s)

n_e = number of single events
 O_{ij} = olefin with carbon number i and isomer index j
 P_i = partial pressure of gas-phase species i (bar)
 $q(i)$ = heat of stabilization of species i (kJ/kmol)
 R_{ij}^+ = olefin with carbon number i and isomer index j
 S° = standard entropy (kJ/kmol K)
 \mathcal{R}_i = net reaction rate for gas-phase species i (kmol/kg of catalyst·h)
 R = gas constant: 8.314 (kJ/kmol K)
 $r_i(j,k)$ = reaction rate for elementary step of type i at j th category and k th reaction (kmol/kg of catalyst·h)
 W = total catalyst mass (kg of catalyst)
 W/F_{MeOH}° = space time of methanol (kg·h/kmol)
 y_i = yield of species i (kg/100 kg of MeOH fed)

Greek Letters

α = transfer coefficient in Evans–Polanyi relation
 v_i = fractional coverage of surface species i
 ΔH^\ddagger = standard enthalpy of activation (kJ/kmol)
 $\Delta H_f^\circ(i)$ = standard enthalpy of formation for species i (kJ/kmol)
 $\Delta H_i(j,k)$ = heat of reaction for elementary step of type i at j th category and k th reaction (kJ/kmol)
 $\Delta H_{\text{pr}}^\circ(i)$ = heat of protonation for gas-phase species i (kJ/kmol)
 ΔG_i = standard Gibbs free energy change of reaction type i (kJ/kmol)
 ΔS^\ddagger = standard entropy of activation (kJ/kmol·K)
 σ = symmetry number
 σ_{gl}^i = global symmetry number of species i

Literature Cited

- (1) Vora, B. V.; Marker, T. L.; Barger, P. T.; Nilsen, H. R.; Kvisle, S.; Fuglerud, T. Economic Route for Natural Gas Conversion to Ethylene and Propylene. *Stud. Surf. Sci. Catal.* **1997**, 107, 87.
- (2) Froment, G. F.; Dehertog, W. J. H.; Marchi, A. J. Zeolite Catalysis in the Conversion of Methanol into Olefins. *Catalysis* **1992**, 9, 1.
- (3) Chen, N. Y.; Reagan, W. J. Evidence of Autocatalysis in Methanol to Hydrocarbon Reactions over Zeolite Catalysts. *J. Catal.* **1979**, 59, 123.
- (4) Schoenfelder, H.; Hinderer, J.; Werther, J.; Keil, F. Methanol to Olefins Prediction of the Performance of a Circulating Fluidized-Bed Reactor on the Basis of Kinetic Experiments in a Fixed-Bed Reactor. *Chem. Eng. Sci.* **1994**, 49, 5377.
- (5) Bos, A. N. R.; Tromp, P. J. J. Conversion of Methanol to Lower Olefins. Kinetic Modeling, Reactor Simulation, and Selection. *Ind. Eng. Chem. Res.* **1995**, 34, 3808.
- (6) Baltanas, M. A.; Van Raemdock, K. K.; Froment, G. F.; Mohedas, S. R. Fundamental Kinetic Modeling of Hydroisomerization & Hydrocracking on Noble-Metal loaded Faujasites. *Ind. Eng. Chem. Res.* **1989**, 28, 899.
- (7) Park, T. Y.; Froment, G. F. Kinetic Modeling of the Methanol to Olefins Process. 1. Model Formulation. *Ind. Eng. Chem. Res.* **2001**, 40, 4172.
- (8) Park, T. Y.; Froment, G. F. Kinetic Modeling of the Methanol to Olefins Process. 2. Experimental Results, Model Discrimination, and Parameter Estimation. *Ind. Eng. Chem. Res.* **2001**, 40, 4187.
- (9) Hutchings, G. J.; Hunter, R. Hydrocarbon Formation from Methanol and Dimethylether: A Review of the Experimental Observation Concerning the Mechanism of Formation of the Primary Products. *Catal. Today* **1990**, 6, 279.
- (10) Park, T. Y.; Froment, G. F. Reaction Rates in the Methanol-to-Olefins Process and their Role in Reactor Design and Operation. Submitted for publication in *Ind. Eng. Chem. Res.*
- (11) Vynckier, E.; Froment, G. F. Modeling of the Kinetics of the Complex Processes based upon Elementary Steps. In *Kinetic and Thermodynamic Lumping of Multicomponent Mixtures*; As-tarita, G., Sandler, S. I., Eds.; Elsevier: Amsterdam, The Netherlands, 1991.
- (12) Feng, W.; Vynckier, E.; Froment, G. F. Single Event Kinetics of Catalytic Cracking. *Ind. Eng. Chem. Res.* **1993**, 32, 2997.
- (13) Svoboda, G. D.; Vynckier, E.; Debrabandere, B.; Froment, G. F. Single Event Rate Parameters for Paraffins Hydrocracking on Pt/US–Y Zeolite. *Ind. Eng. Chem. Res.* **1995**, 34, 3793.
- (14) Baltanas, M. A.; Froment, G. F. Computer Generation of Reaction Networks and Calculation of Product Distributions in the Hydroisomerization and Hydrocracking of Paraffins on Pt-containing Bifunctional Catalysts. *Comput. Chem. Eng.* **1985**, 9, 71.
- (15) Dewachtere, N.; Santaella, F.; Froment, G. F. Application of a Single Event Kinetic Model in the Simulation of an Industrial Riser Reactor for the Catalytic Cracking of Vacuum Gas Oil. *Chem. Eng. Sci.* **1999**, 54, 3653.
- (16) Evans, M.; Polanyi, M. Inertia and Driving Force of Chemical Reactions. *Trans. Faraday Soc.* **1938**, 31, 11.
- (17) Abraha, M. Methanol to Olefins: Enhancing Selectivity to Ethylene and Propylene using SAPO-34 and Modified SAPO-34. Ph.D. Dissertation, Chemical Engineering Department, Texas A & M University, 2001.
- (18) Boudart, M.; Mears, D. E.; Vannice, M. A. *Ind. Chim. Belg.* **1967**, 32, 281.
- (19) Park, T. Y.; Froment, G. F. A Hybrid Genetic Algorithm for the Estimation of the Parameters in Detailed Kinetic Models. *Comput. Chem. Eng.* **1998**, 22, S103.
- (20) Hammond, G. S. *J. Am. Chem. Soc.* **1955**, 77, 334.
- (21) Marchi, A. J.; Froment, G. F. Catalytic Conversion of Methanol to Light Alkenes on SAPO Molecular Sieves. *Appl. Catal.* **1991**, 71, 139.
- (22) Froment, G. F.; Bischoff, K. B. *Chemical Reactor Analysis and Design*, 2nd ed.; John Wiley: New York, 1990.

Received for review January 29, 2004
 Revised manuscript received May 21, 2004
 Accepted May 25, 2004

IE040041U